ISSN 1063-7761, Journal of Experimental and Theoretical Physics, 2010, Vol. 111, No. 1, pp. 104–113. © Pleiades Publishing, Inc., 2010.
Original Russian Text © S.G. Ovchinnikov, M.M. Korshunov, L.P. Kozeeva, A.N. Lavrov, 2010, published in Zhurnal Éksperimental'noĭ i Teoreticheskoĭ Fiziki, 2010, Vol. 138, No. 1, pp. 115–125.

ELECTRONIC PROPERTIES OF SOLID

Peculiarity of Interrelation between Electronic and Magnetic Properties of HTSC Cuprates Associated with Short-Range Antiferromagnetic Order

S. G. Ovchinnikov[a, b, *], M. M. Korshunov[a, c], L. P. Kozeeva[d], and A. N. Lavrov[d]

[a] *Kirenskii Institute of Physics, Siberian Branch, Russian Academy of Sciences, Krasnoyarsk, 660036 Russia*
[b] *Siberian Federal University, Krasnoyarsk, 660041 Russia*
[c] *Department of Physics, University of Florida, Gainesville, Florida, 32611 USA*
[d] *Nikolaev Institute of Inorganic Chemistry, Siberian Branch, Russian Academy of Sciences, Novosibirsk, 630090 Russia*
**e-mail: sgo@iph.krasn.ru*

Received December 22, 2009

Abstract—We report on the results of measurements of anisotropic resistivity of $RBa_2Cu_3O_{6+x}$ (R = Tm, Lu) high-temperature superconducting single crystals in a wide range of doping levels, indicating a nontrivial effect of magnetic order on the electronic properties of cuprates. In particular, our results visually demonstrate the crossover from the state with moderate anisotropy of resistivity $\rho_c/\rho_{ab} \sim 30$ to a strongly anisotropic state with $\rho_c/\rho_{ab} \sim 7 \times 10^3$ upon cooling as well as upon a decrease in the hole concentration in the CuO_2 planes. It is also shown that anisotropy is sensitive to the magnetic state of CuO_2 planes and attains its maximum value after the establishment of the long-range antiferromagnetic order. The results are discussed in the framework of the theory based on the t–t'–t''–J model of CuO_2 layers taking into account strong electron correlations and short-range magnetic order. In this theory, anomalies of spin correlators and Fermi surface topology for a critical hole concentration of $p^* \approx 0.24$ are demonstrated. The concentration dependence of the charge carrier energy indicates partial suppression of energy due to the emergence of a pseudogap at $p < p^*$. This theory explains both the experimentally observed sensitivity of anisotropy in conductivity to the establishment of the antiferromagnetic order and the absence of anomalies in the temperature dependence of resistivity $\rho_{ab}(T)$ in the vicinity of the Néel temperature.

DOI: 10.1134/S1063776110070101

1. INTRODUCTION

The interrelation between variations in the electric and magnetic properties is often encountered in transition metal compounds. The most visual example is a metal–insulator transition with the formation of spin density waves (e.g., NiS or V_2O_3 [1]). For this reason, the absence of changes in resistivity $\rho_{ab}(T)$ of weakly doped nonsuperconducting cuprates [2–4] upon a transition through the Néel point T_N in experiments is sometimes interpreted as the absence of a strong coupling between charge carriers and the magnetic subsystems. Here, we give an alternative interpretation, in which the coupling of charge carriers with the spin system exists and is strong, while the absence of changes in ρ_{ab} in the vicinity of T_N is explained by specific features of the magnetic state of quasi-two-dimensional antiferromagnets. We also report on new experimental results on anisotropic transport properties of $RBa_2Cu_3O_{6+x}$ (R = Tm, Lu) single crystals, indicating the effect of the magnetic structure on the electronic properties at temperatures corresponding to the existence of long-range antiferromagnetic (AFM) order as well as at $T > T_N$. The article has the following structure. In Section 2, the interrelation between the electronic and magnetic structures and the peculiarities of quasi-two-dimensional antiferromagnetism in cuprates are considered qualitatively. In Section 3, experimental data on intra- and interplanar conductivity of $RBa_2Cu_3O_{6+x}$ (R = Tm, Lu) single crystals are considered in a wide range of hole concentrations. In Section 4, the electronic properties are analyzed with allowance for the short-range magnetic order and the pseudogap and are compared qualitatively with experiment.

2. SPECIFIC FEATURES OF MAGNETISM IN QUASI-TWO-DIMENSIONAL CUPRATES

It is well known that a metal with a Fermi surface satisfying the nesting condition is unstable to the transition to the state of a charge- or spin-density wave. In a particular case of an antiferromagnetic spin-density wave, the dielectric state is formed below the Néel point [5, 6]. In the Hubbard model, which is often used for describing the electronic structure of transition metal compounds, such a band mechanism of the metal–insulator transition takes place in the weak cor-

relation limit $U \ll W$, where U is the Hubbard parameter and W is the band half-width. In the opposite limit of strong correlations ($U \gg W$), the interrelation between electronic and magnetic properties becomes even stronger. Even in the absence of charge carriers in an undoped Mott–Hubbard dielectric, the exchange interaction between neighboring spins J_{ij} is formed by virtual electron jumps t_{ij} from the ith site to the jth site and back, $J = 2t^2/U$. Doped electrons (or holes) hopping from one site to another against the background of the antiferromagnetic structure have a jump amplitude depending on spin correlators $C_{ij} = \langle \mathbf{S}_i \cdot \mathbf{S}_j \rangle$ of neighboring spins [7]. This is the main mechanism of interrelation between the electronic and magnetic properties in the strong correlation mode. A more rigorous calculation of the electron Green's function shows that the mass operator in the Hubbard model is determined by the correlation functions of spin, charge, and pair fluctuations [8, 9]. As a result, we can expect a change in the electronic structure as a result of transition from the antiferromagnetic to the paramagnetic phase, in which spin correlators disappear, either to the metal state (in the weak correlation mode), as in NiS, or to the paramagnetic Mott–Hubbard dielectric. An example of the latter situation is $LaTiO_3$, in which the dielectric properties are preserved above T_N also, but the temperature dependence $\rho(T)$ has a kink at the Néel point [10]. The smooth temperature dependence of ρ_{ab} in cuprates in the vicinity of the Néel point [2–4] and the absence of qualitative changes in $\sigma_{ab}(T)$ upon a transition from compositions with the paramagnetic state to those with a long-range AFM order [2–4] appear even more surprising.

What is the difference between the variation of the magnetic structure upon a transition through the Néel point in La_2CuO_4, $YBa_2Cu_3O_6$, and other undoped cuprates and that in NiS or $LaTiO_3$? In the latter case, the magnetic system is three-dimensional, while in cuprates it is quasi-two-dimensional. In a 3D magnet, the range of strong spin fluctuations above T_N is narrow, while the behavior of these fluctuations in a quasi-two-dimensional antiferromagnet is much more complicated. These systems are characterized by two energy scales: strong exchange in the plane ($J \sim 0.1$ eV) and weak exchange between the planes ($J' \sim (10^{-4}$–$10^{-5})J$) (or anisotropy in the plane of the same order of magnitude, which is equivalent as regards the formation of the 3D long-range antiferromagnetic order). It is well known that, in the isotropic Heisenberg model, the Néel temperature in a 2D system must be zero in accordance with the Mermin–Wagner theorem. Anisotropy and interplanar exchange stabilize the 3D antiferromagnetic order in La_2CuO_4 with Néel temperature $T_N \sim J/\ln(J/J')$ [11]. Above the Néel point, the long-range order (correlations between CuO_2 layers) is broken, while strong exchange J in the CuO_2 plane preserves antiferromagnetic correlations (short-range order) up to temperatures $T \sim J \sim 1000$ K. Neutronographic measurements show that the antiferromagnetic correlation length ξ decreases rather slowly upon an increase in the doping level, $\xi \propto x^{-1/2}$ [12]. Since the mean free path l of charge carriers is close to or even smaller than ξ in a wide range of temperatures and doping levels, holes move in the antiferromagnetic surrounding most of their lifetime. Time fluctuations of the short-range order at low temperatures are practically frozen. For example, at $T \leq 10$ K, the characteristic lifetime of an antiferromagnetic cluster of size ξ is 10^{-9} s, which is much larger than the characteristic electron lifetime of 10^{-13} s [13]. Therefore, the main contribution to the formation of the electronic structure of carriers in a strongly correlated system of electrons in the CuO_2 layer comes from quasi-static antiferromagnetic short-range correlations. The changes in the electronic structure upon a transition through the Néel point are insignificant since (by virtue of the scaling condition $l \ll \xi$) it is immaterial for moving holes whether the correlation length is infinitely large in the case of long-range order or is 20 nm. We cannot state that there are no variations at all: scattering of holes from space and time inhomogeneities of the magnetic structure leads to anisotropic damping of carriers responsible for spreading of a part of the hole pocket on the Fermi surface [9, 14, 15] and the formation of the finite Fermi arches observed in ARPES experiments [16].

3. TRANSPORT PROPERTIES OF SINGLE CRYSTALS

One of the most visual manifestations of the peculiar electronic states of HTSC cuprates is the contrasting behavior of the electron transport along CuO_2 planes and between them. In this case, metal-type conductivity $\sigma_{ab}(T)$ can be combined with the activation behavior of $\sigma_c(T)$ [2–4, 17, 18], and the conductivity anomalies associated with antiferromagnetic ordering are manifested only in the interplanar direction [2–4, 18]. A comprehensive explanation of such a behavior has not been obtained as yet; in particular, this is due to the lack of systematic experimental data on conductivity anisotropy as a function of the doping level for most HTSC cuprate families. In this connection, we performed detailed measurements of anisotropic resistivity of $RBa_2Cu_3O_{6+x}$ (R = Tm, Lu) single crystals in the composition range from a weakly doped antiferromagnet to an optimally doped superconductor. The techniques for growing single crystals, setting the required concentration of oxygen, and precision measurement of resistivity components were described in detail in our previous publications [2, 3]. Since the behavior of $TmBa_2Cu_3O_{6+x}$ and $LuBa_2Cu_3O_{6+x}$ single crystals is qualitatively the same, the results on these compounds will be distinguished in the text only in the cases where it is impor-

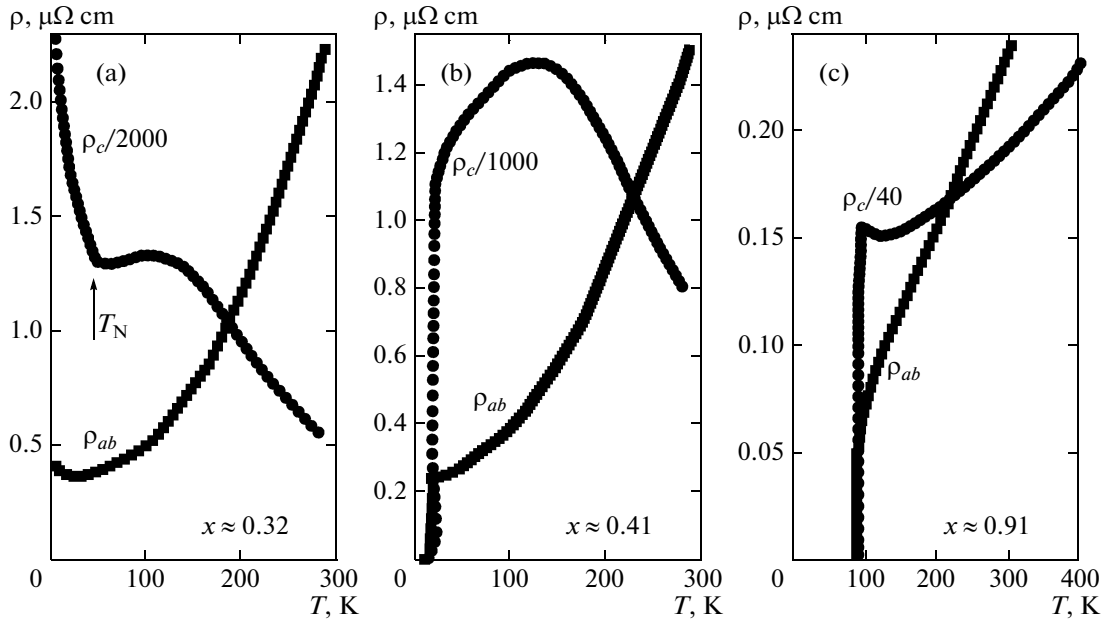

Fig. 1. Temperature dependences of anisotropic resistivity of $RBa_2Cu_3O_{6+x}$ (R = Tm, Lu) single crystals in various doping level ranges: for (a) a weakly doped nonsuperconducting compound with $T_N \approx 43$ K; (b) a weakly doped superconducting compound with $T_C \approx 19$ K, and (c) approximately optimally doped crystals with $T_C \approx 90$ K.

tant that the entire set of measurements is made on the same crystal.

Figure 1 shows the characteristic temperature dependences of anisotropic resistivity for three doping level ranges. It can immediately be seen that the resistivity component along CuO_2 planes exhibits a practically invariable behavior: the $\rho_{ab}(T)$ curves are similar to one another, although the doping level range under investigation extends from the nonsuperconducting antiferromagnet to the optimally doped superconductor. The only qualitative change (if we disregard the superconducting transition) is a slight variation of the curvature of the $\rho_{ab}(T)$ dependence. The absolute value of ρ_{ab} in the normal state changes only by a factor of 6–9 (depending on temperature) upon a change in the oxygen concentration x from 0.32 to 0.91, corresponding to a change in the hole concentration p in the CuO_2 layer by a factor of 4–5 (from $p \approx 3.5$–4% to 17%) [4, 19]. Consequently, the increase in the conductivity normalized to the hole concentration upon a transition from antiferromagnetic compounds to the optimally doped superconductor is only by a factor of 1.5–2. If we recall that the additional conductivity of layers formed by CuO_x chains for an oxygen concentration of $x \approx 0.9$ becomes comparable with the conductivity of CuO_2 planes, the increase in the carrier mobility is bounded from above by only a few tens of percent, which is close to the errors of resistivity and carrier concentration measurements. Thus, the type of electron transport along CuO_2 planes weakly depends on the doping level. Only the scaling of carrier concentration and intraplanar conductivity takes place, which confirms the conclusions [4] about the weak dependence of the hole mobility in CuO_2 planes on the doping level.

The behavior of interplanar resistivity $\rho_c(T)$ in Fig. 1 is much more complicated. The form of the $\rho_c(T)$ dependence changes from the quasi-metallic behavior at the maximal doping levels to a complex dome-shaped curve for weakly doped compounds, which is supplemented with a sharp kink of the curve upon a transition to the state with the long-range antiferromagnetic order below the Néel temperature T_N (marked by the arrow in Fig. 1) [2, 3]. The sharp increase in ρ_c below the Néel temperature in the absence of singularities on the $\rho_{ab}(T)$ curve appears more unusual [2–4]. The sharp increase in the value of ρ_c upon a transition to the AFM state unambiguously indicates a significant role of the spin order in the interplanar electron transport.

A visual idea of the evolution of resistivity anisotropy can be gained from systematic data on ρ_c/ρ_{ab} obtained for the same pair of samples cut from the same $TmBa_2Cu_3O_{6+x}$ single crystal (Fig. 2). The temperature dependence of ρ_c/ρ_{ab} is much simpler than the behavior of the single ρ_c component. It can be seen from Fig. 2 that the resistivity anisotropy smoothly increases from approximately 30 (see also Fig. 1c) to approximately 7000–8000 both upon a decrease in temperature and upon a decrease in the doping level at a fixed temperature. The variation of anisotropy has the form of a crossover between two selected states with moderate and strong electron anisotropy. Although the range of AFM compounds is not repre-

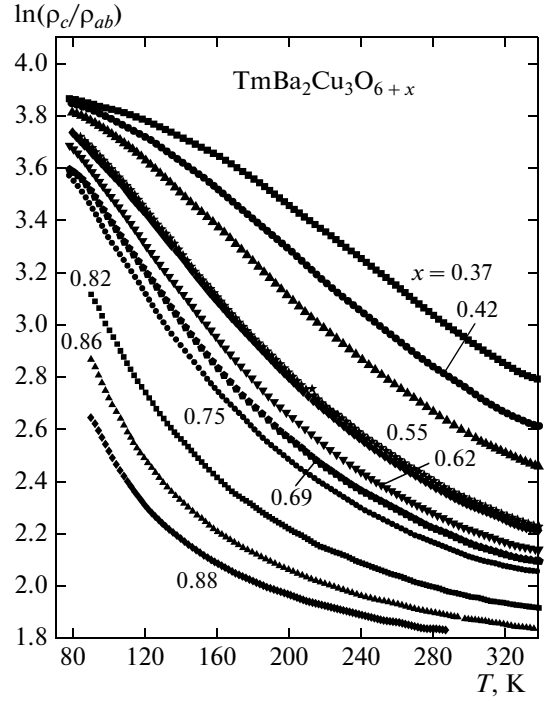

Fig. 2. Temperature dependence of resistivity anisotropy ρ_c/ρ_{ab} of $TmBa_2Cu_3O_{6+x}$ single crystals with various oxygen concentrations. All values of resistivity components $\rho_c(T)$ and $\rho_{ab}(T)$ were obtained for the same pair of samples cut from the same crystal and subjected to simultaneous annealing. Measurements were taken after relaxation of the crystals at room temperature leading to oxygen ordering in CuO_x chain layers.

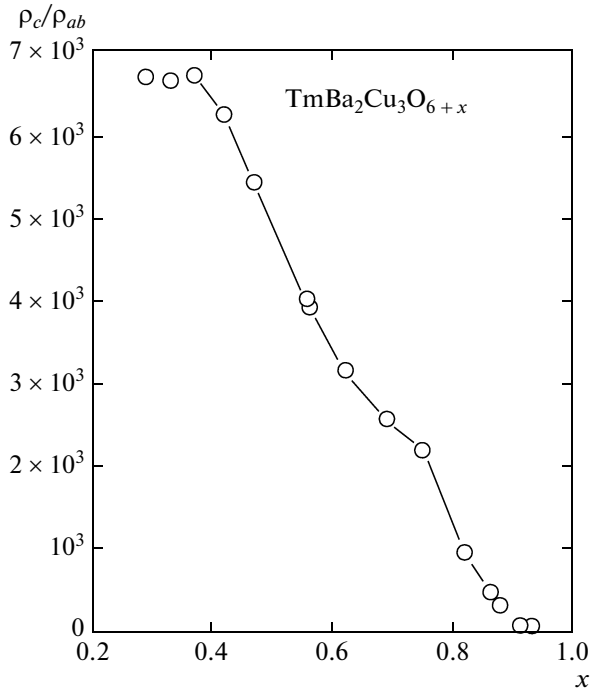

Fig. 3. Dependence of resistivity anisotropy ρ_c/ρ_{ab} of $TmBa_2Cu_3O_{6+x}$ single crystals at $T = 100$ K on the oxygen concentration.

sented in Fig. 2, it can easily be seen from Fig. 1 that a transition to the AFM state leads to an additional sharp increase in anisotropy [3]. The absolute value of anisotropy ρ_c/ρ_{ab} at $T = 100$ K varied almost linearly upon an increase in the hole concentration (Fig. 3) and is saturated in the above-mentioned regions with a moderate (about 30–50) and strong (about 10^4) anisotropy.

The effect of spin AFM ordering on the conductivity anisotropy is clearly manifested upon a transition through the Néel temperature. However, the effect of spin correlations on the electron transport in the range of superconducting compositions is more important for explaining the HTSC origin. Indeed, dynamic AFM correlations are preserved in an extremely broad range of compositions and temperatures [12] (Fig. 4a) and can be responsible not only for the clearly manifested anomaly in $\rho_c(T)$ at T_N but also for the observed smooth increase in the resistivity anomaly upon a decrease in the carrier concentration and in the vicinity of the range of the AFM order. This question could be clarified by shifting the Néel temperature and changing the scale of AFM correlations. Such a change (albeit small) is indeed possible for $RBa_2Cu_3O_{6+x}$ compounds. It was demonstrated recently [20] that the application of a strong magnetic field stabilizes AFM correlations and increases the Néel temperature. Although the mechanism of this effect is not completely clear, one of its possible explanations is the additional anisotropy introduced into the spin system by the magnetic field. This additional anisotropy enhances AFM correlations and stabilizes the long-range order analogously to magnetic-crystal anisotropy or interplanar spin interaction J'. The long-range AFM order is established in cuprates when J' integrated over the correlation volume $(J'\xi_{ab}^2)$ becomes equal to k_BT. The additional magnetic anisotropy introduced by the magnetic field is also integrated over the AFM correlation volume and competes with thermal disordering. Obviously, the strongest effect of the magnetic field must be observed near T_N, where correlations are strong enough, while the effect of the magnetic field upon an increase in temperature or in the doping level decreases approximately in proportion to $[\xi_{ab}(T, p)]^2/k_BT$. The enhancement of AFM correlations induced by the applied magnetic field may in turn affect the interplanar transport; this can be observed in magnetoresistance measurements. Such measurements performed in [20, 21] revealed that the magnetic field indeed induces a substantial positive magnetoresistance $\Delta\rho_c$ and, accordingly, increases anisotropy ρ_c/ρ_{ab}; the range of temperatures in which this effect is observed is not bounded by the region of long-range AFM order

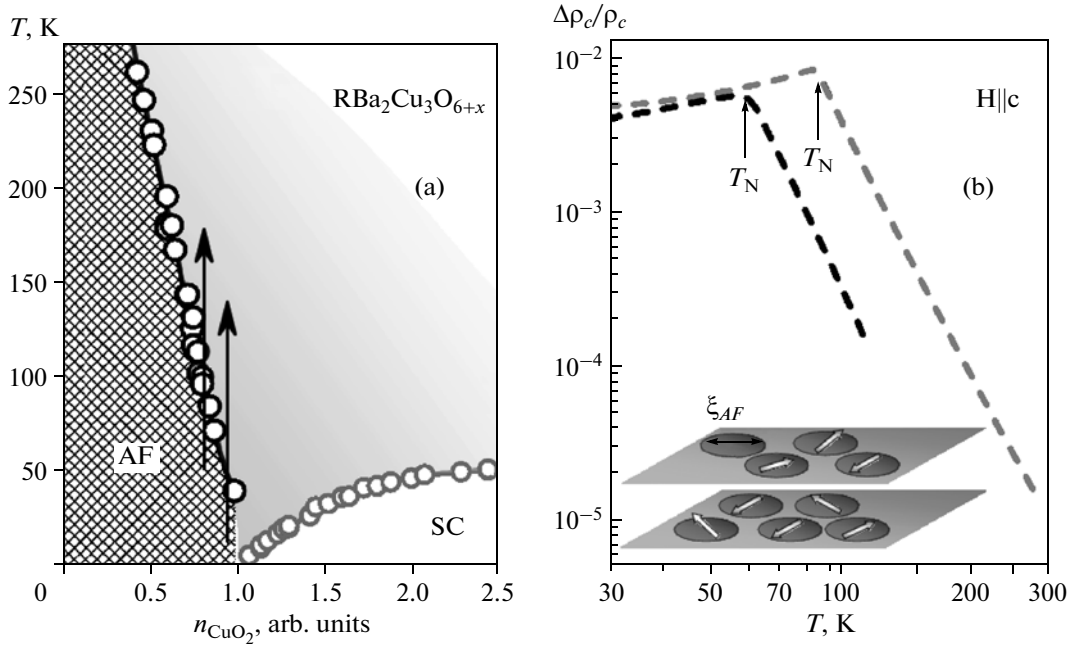

Fig. 4. (a) Phase diagram of $RBa_2Cu_3O_{6+x}$ compounds in the range of antiferromagnet–superconductor transformation [3] as a function of carrier concentration n_{CuO_2} with its relative values determined from the data on the conductivity in CuO_2 planes. The threshold concentration at which superconductivity appears is taken as unity. The shaded part on the phase diagram above T_N and T_C schematically illustrates the range of strong dynamic AFM correlations in CuO_2 planes. Arrows indicate the states for which magnetoresistance data are given in (b) showing the temperature dependence of the interplanar magnetoresistance $\Delta\rho_c/\rho_c$ of $RBa_2Cu_3O_{6+x}$ single crystals in a magnetic field **H** ∥ **c** borrowed from [21]. The inset illustrates the magnetic state of $RBa_2Cu_3O_{6+x}$ in the range above T_N: two-dimensional antiferromagnetic correlations have magnitude $\xi_{AF}(T)$ in CuO_2 planes and fluctuating direction of the sublattice magnetization (shown by arrows).

and extends to high temperatures (Fig. 4b). The spin origin of the observed magnetoresistance can easily be verified by slightly changing the hole concentration and, accordingly, by shifting the Néel temperature. It can be seen from Fig. 4 that, upon a displacement of T_N, the entire magnetoresistance curve exhibits a parallel shift, which confirms the interrelation between the magnetoresistance in the entire temperature range under investigation and the AFM ordering. Thus, AFM correlations indeed affect the interplanar transport and resistivity anisotropy not only in the region of AFM order but also in wide ranges of temperatures and compositions, in which strong AFM correlations are preserved.

4. ELECTRONIC PROPERTIES IN THE PSEUDOGAP STATE

On account of the interrelation between charge carriers and magnetic moments, the electronic and magnetic structures must be calculated self-consistently for each point (x, T) on the phase diagram. Due to strong electron correlations, we must take into account in our calculations the prohibition on the occupation of two-particle states; for this purpose, it is convenient to use Hubbard X operators $X^{pq} = |p\rangle\langle q|$. Here, $|p\rangle$ and $\langle q|$ are local states $|\sigma\rangle$ with a single hole and spin $\sigma = \pm 1/2$, as well as the Zhang–Rice singlet $|S\rangle$. The exclusion of double filling for hole-type cuprates indicates that two-electron states $d^{10}p^6$ (hole vacuum $|0\rangle$) are excluded from the local basis of the Hubbard model. In spite of the complexity of the algebra of X-operators as compared to the conventional Fermi or Bose operators, their application guarantees that two-particle prohibition is taken into account exactly in any approximation in contrast to the slave boson method. The microscopic multiband p–d model taking into account all orbitals of copper and oxygen, as well as strong Coulomb interactions between electrons, is used for deriving the t–t'–t''–J^* model with jumps t, t', and t'' to the first, second, and third neighbors and with the J exchange [22]. The asterisk indicates that we take into account three-center correlated jumps whose amplitude is also J.

Here, it is not expedient to write Green's functions and the mass operator for holes, which are defined by the spin ($C_{0n} = \langle S_0^+ S_n^- \rangle$) and kinetic ($K_{0n} = \langle X_0^{S\bar{\sigma}} X_n^{\bar{\sigma}S} \rangle$) correlation-induced fluctuations. For the lower Hubbard band determined by operator $X^{0\sigma}$ and corresponding to the bottom of the conduction band, the

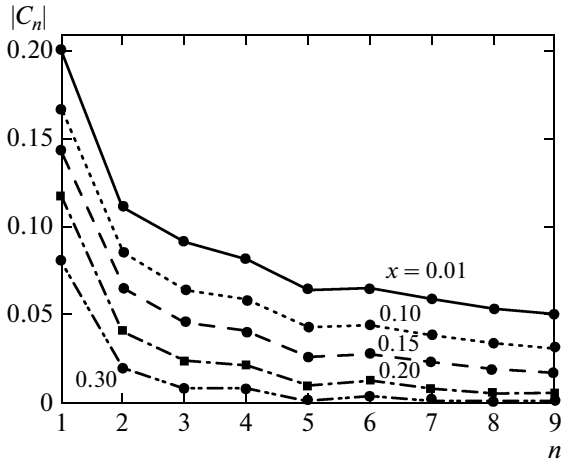

Fig. 5. Decreasing spin correlation functions C_{0n} for various doping hole concentrations x and numbers n of coordination spheres. For $n = 2, 3, 5, 7$, and 9, correlations are positive (within one sublattice), while for $n = 1, 4, 6$, and 8, correlations are negative (between different sublattices).

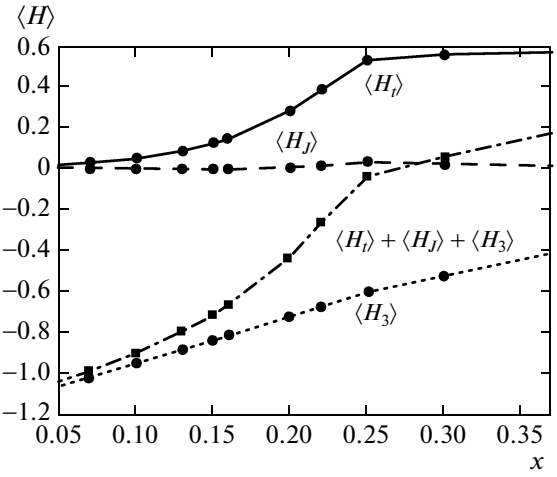

Fig. 6. Concentration dependence of the kinetic, potential, and total energies in the t–t'–t''–J^* model in the state of an isotropic spin liquid. The kink and partial suppression of the kinetic energy below $x_c = 0.24$ correspond to the formation of the pseudogap state.

procedure and results of calculations are described in [22, 23]. Analogous calculations for the valence band of interest to us in the case of hole doping, which coincides with the upper Hubbard band in the hole representation and is described by operator $X^{\bar{\sigma}S}$, are given in [24]. In the development of the research in [24], we consider new results required for the discussion of experimental data.

The magnetic structure with a short-range antiferromagnetic order is described in the approximation of an isotropic spin liquid, in which all spin components have identical correlation functions $\langle S_0^x S_n^x \rangle = \langle S_0^y S_n^y \rangle = \langle S_0^z S_n^z \rangle = C_{0n}/2$. These functions can be determined from the spin Green's function $\langle\langle S_i^+ | S_j^- \rangle\rangle$ using the method developed in [22, 23, 25, 26]. Kinetic correlators K_{0n} and the chemical potential can be expressed in terms of the hole Green's function $\langle\langle X_i^{\bar{\sigma}S} | X_j^{S\bar{\sigma}} \rangle\rangle$. For each doping level x with total hole concentration $n_h = 1 + x$, the correlators and the chemical potential are determined self-consistently (i.e., the changes in the electronic and magnetic structures in the theory are interrelated). Figure 5 shows the moduli of the spin correlation functions depending on the number of the nth coordination sphere up to $n \le 9$ for various values of x. It should be noted that the correlations are antiferromagnetic; i.e., C_{0n} is negative for the alien sublattice ($n = 1, 4, 6, 8$) and positive for its own sublattice ($n = 2, 3, 5, 7, 9$). It can be seen that, in the weak doping region, spin correlations decrease quite slowly. For strongly doped compositions with $x = 0.3$, correlations take place only between the nearest neighbors; precisely such a behavior of spins in a paramagnet is expected. The composition with $x = 0.20$ still shows the traces of the short-range order, although the doping level is higher than optimal. It can be seen from the concentration dependence of correlators C_{0n} that a critical point $x_c = 0.24$ exists, at which C_{01} has a kink, while correlators with larger numbers vanish for $x > x_c$. Point x_c is close to the critical value corresponding to the emergence of a pseudogap $p^* = 0.24$.

To determine the role of critical point x_c, we calculated the concentration dependence of the total energy $\langle H \rangle$ (Fig. 6) and its partial components: kinetic energy $\langle H_t \rangle$, potential energy $\langle H_J \rangle$, and correction to energy $\langle H_3 \rangle$ from three-center correlated jumps. The energy origin is set at the mean value of the one-site part of the Hamiltonian,

$$\langle H_0 \rangle = \sum_{i\sigma} (\varepsilon - \mu) \langle n_{i\sigma} \rangle.$$

The three-center terms are important for the formation of the superconducting state with the $d_{x^2-y^2}$ symmetry since their amplitude is determined by exchange parameter J [27]. The resultant smallness of their contribution to energy is in conformity with the result of exact diagonalization of finite one-dimensional and two-dimensional clusters [28]. Potential energy $\langle H_J \rangle$ varies with the hole concentration almost linearly with a small kink at critical point x_c. The critical point is manifested most strongly in the kinetic energy of carriers. Above x_c, the dependence is linear (approximately proportional to $1 + x$), which is typical of a 2D electron gas with mean energy $\bar{\varepsilon} \sim \varepsilon_F \sim n_h = 1 + x$. The continuation of this dependence to the left of the crit-

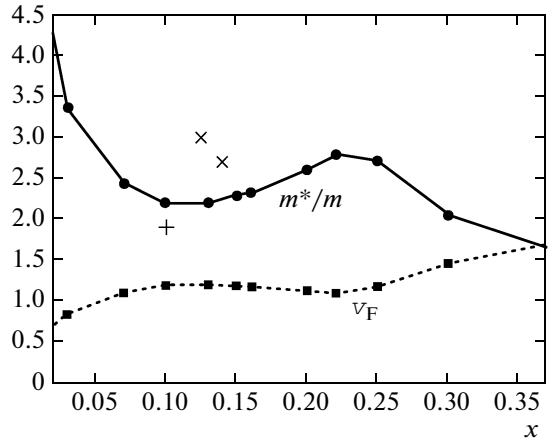

Fig. 7. Concentration dependences of effective mass m^*/m_0 and velocity v_F at the Fermi level in the nodal direction [1, 2]: experimental values of the effective mass from the data on quantum oscillations are marked by symbols + for $YBa_2Cu_3O_{6.5}$ [30] and × for $YBa_2Cu_3O_8$ [31, 32].

ical point shows that the kinetic energy for $x < x_c$ is lower than that expected for a free electron gas. We attribute this decrease in the energy to the formation of a pseudogap in the vicinity of the Fermi level, as a result of which some electron states make zero contribution to the energy. Thus, the coincidence of our critical point x_c with point p^* is not accidental; this point corresponds to origination of a pseudogap at $T = 0$ below $x_c = p^*$. The concentration dependence of the kinetic energy is described by the relation

$$\frac{E_{\rm kin}(p)}{E_{\rm kin}(p^*)} = \exp\left\{-\frac{4E_g(p)}{J}\right\},$$

in which the pseudogap is $E_g(p) = J(1 - p/p^*)$. In our theory, the pseudogap appears due to enhancement of the short-range antiferromagnetic order upon a decrease in the doping concentration and is close to the spin-fluctuation origin considered in [15, 29].

The characteristics of charge carriers such as effective mass m^* and velocity v_F at the Fermi level are important for analysis of transport experiments. It should be noted that the variations of these quantities depicted in Fig. 7 in a wide range of concentration from weakly doped to strongly doped compositions are insignificant. Small changes in the Fermi velocity were detected by the ARPES methods [33], while variations in the effective mass of carriers were determined from analysis of experimental data on transport and optical properties [4, 34]; our calculations are in qualitative agreement with the conclusions drawn in [4, 34].

The electrical conductivity in strongly correlated systems has not been calculated as thoroughly as the electronic structure with evolution of the Fermi surface [24]. Instead of the results of such calculations, we will consider a rougher qualitative estimate based on analysis of different mechanisms of transport along and across the CuO_2 plane. Hopping of holes in the plane mainly occurs in each AFM cluster in view of the condition $l \ll \xi$. Such jumps are coherent in the sense that a doped antiferromagnet is a metal with a definite Fermi surface (even if some part of it does not participate in conduction due to the formation of the pseudogap, the remaining Fermi arches ensure metal-type conduction). At the same time, jumps along the c axis always occur between different AFM clusters (i.e., incoherently). This incoherence will be taken into account as follows. Usually, the electrical conductivity is calculated using the relaxation time approximation for the nonequilibrium part of the Fermi distribution function $g_k = f_k - f_k^0$ (where f_k and f_k^0 are the nonequilibrium and equilibrium functions):

$$-\frac{\partial f_k}{\partial t} = -\frac{\partial g_k}{\partial t} = \frac{g}{\tau}. \quad (1)$$

We will use this formula and the conductivity tensor of the familiar type

$$\sigma_{ij} = \frac{e^2\tau}{4\pi^3\hbar}\iint v_{k_i} v_{k_i}\left(-\frac{\partial f^0}{\partial \varepsilon}\right)d\varepsilon\frac{dS}{|\mathbf{v}_k|} \quad (2)$$

following from it for describing the transport in the a, b plane. Here, $\mathbf{v}_k = \nabla_k\varepsilon(k)/\hbar$ and dS is the constant-energy surface area element (in the case of a 2D plane, it is an element of an arc of the constant-energy curve). The incoherence of the jump along the c axis will be taken into account using the fact that the reciprocal relaxation time is of the activation type:

$$1/\tau_c = 1/\tau\exp\{-E_g/kT\}, \quad (3)$$

where $E_g(k, p) = E_g(p)\varphi_k$ is the pseudogap depending on the wavevectors in the a, b plane and on the doping level,

$$E_g(p) = J\left(1 - \frac{p}{p^*}\right),$$
$$\varphi_k = \frac{1}{2}(\cos k_x a - \cos k_y a). \quad (4)$$

In fact, expression (3) is our hypothesis based on the difference in the hopping mechanisms in the a, b plane and in the c direction. As regards the angular dependence of the form of $d_{x^2-y^2}$ (4), it was established experimentally by the ARPES methods [35–38] and was derived theoretically in [39] for weakly doped AFM cuprates. The gap amplitude in the form $E_g(p) = J(1 - p/p^*)$ was proposed for analyzing the temperature and concentration dependences of the electronic entropy and heat capacity [37]; we obtained the same concentration dependence for the kinetic energy (Fig. 6).

In calculating conductivity by formula (2), we must integrate, as usual, over the Fermi surface:

$$-\frac{\partial f^0}{\partial \varepsilon} = \delta(\varepsilon_k - \mu). \quad (5)$$

This gives the following expression for resistivity ratio $y = \rho_c/\rho_{ab}$:

$$y = \int k_x k_y \delta(\varepsilon_k - \mu) dk_x k_y \times \left[\int k_z^2 \exp\left\{ -\frac{E_g(p)}{2kT}(\cos k_x a - \cos k_y a) \times \delta(\varepsilon_k - \mu) dk_x k_y \right\} \right]^{-1}. \quad (6)$$

In the doping range $p \geq p_{\text{opt}}$, where $p_{\text{opt}} \approx 0.16$ is the optimal doping level, the Fermi surface is large. To obtain a simple estimate, we approximate it by the expression

$$\cos k_x a + \cos k_y a = 0. \quad (7)$$

This gives the following expression for the conductivity anisotropy:

$$y = \frac{\sigma_{ab}}{\sigma_{c0} \int_{-\pi.2}^{\pi/2} \exp\left(-\frac{E_g(p)}{kT}\cos x\right) dx} = \frac{y_0}{I_0(a)}. \quad (8)$$

Here, σ_{c0} is the conductivity along the c axis in the absence of the pseudogap for $p > p^*$, $I_0(a)$ is the Bessel function of the imaginary argument, $y_0 = \sigma_{ab}/\pi\sigma_{c0}$, and $a = E_g(p)/kT$. It should be noted that formula (8) cannot be treated as the theory of resistivity anisotropy; it was derived with a number of rough simplifications and will be used only for qualitative comparison with experiment.

It should be noted that the simplified estimates of anisotropy considered above do not allow us to describe the temperature dependences of ρ_{ab} and ρ_c separately. For this purpose, we must take into account explicitly the scattering of carriers from spin fluctuations. This was done earlier by many authors using the phenomenological approach of a nearly antiferromagnetic Fermi liquid [40–44] as well as microscopic approaches taking strong electron correlations into account [45–48]. This makes it possible to describe the linear temperature dependence of resistivity of optimally doped cuprates. In calculating the resistivity ratio ρ_c/ρ_{ab}, such power corrections are canceled out, and exponential dependence (3), which is associated with the emergence of a pseudogap, plays the major role in the effects discussed here.

Formula (8) used for comparison with experiment contains an empirical parameter y_0. The pseudogap parameters are calculated ab initio from the microscopic theory [24]: $J \sim 1600$ K and $p^* = 0.24$. Figure 8 shows a series of temperature dependences of ln y for various values of the doping element concentration. Parameter $y_0 = 35$. At high temperatures, the entire set of experimental curves for various concentrations can be described by formula (8). As the doping level decreases, the discrepancy between the theory and experiment becomes stronger, which we attribute to the roughness of the description of the Fermi surface. Indeed, Eq. (7) fails to describe small pockets and arches, which are known for weakly doped compositions. Comparison of the concentration dependence of ρ_{ab} with ARPES data [38] shows that the variation of resistivity upon a decrease in p is in good agreement with the decrease in the length of Fermi arches preserved in the vicinity of diagonals $(0, 0)$–(π, π) and with the decrease in the spectral weight in the vicinity of these points. Thus, the conductivity in the CuO_2 layers is associated with length L of the arch.

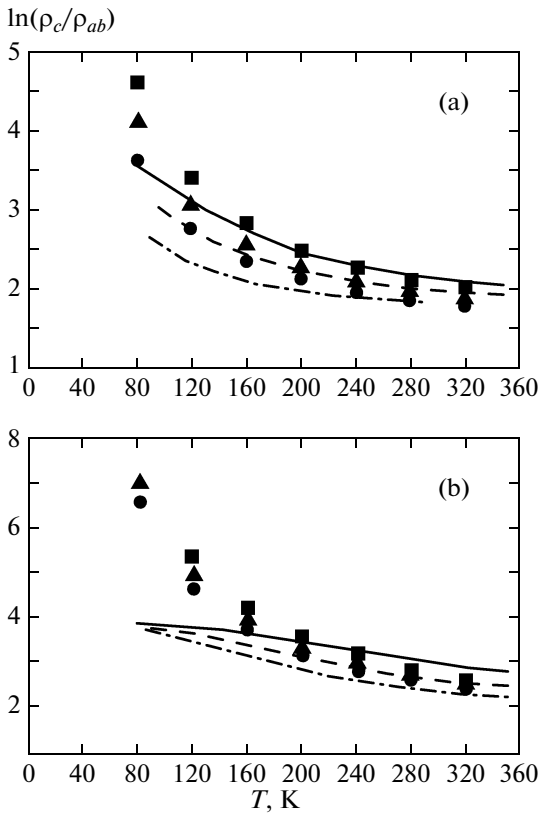

Fig. 8. Comparison of experimental and theoretical dependences of resistivity anisotropy for compounds (a) with nearly optimal doping level and (b) with a low doping level: (a) $p = 0.13$ (solid curve, ■); 0.145 (dashed curve, ▲); 0.16 (dot-and-dash curve, ●); (b) 0.045 (solid curve, ■); 0.06 (dashed curve, ▲); 0.075 (dot-and-dash curve, ●).

Upon a decrease in temperature, the discrepancy between the result of calculation by formula (8) and experiment increases for the same reason as in the case of decreasing doping level: AFM correlations increase, which changes the band structure and the Fermi sur-

face. Analysis of a more general formula (6) for $T \longrightarrow 0$ indicates the boundedness of the ratio ρ_c/ρ_{ab}. Indeed, the exponential factor for $T \longrightarrow 0$ determines the situation where the contribution to the integral comes only from those regions in the k space in which $\varphi_k = 0$. These are nodal directions $k_x = \pm k_y$. It is this truncation of the integral due to the pseudogap that leads to boundedness of ρ_c/ρ_{ab} for $T \longrightarrow 0$.

5. CONCLUSIONS

The theory of the electronic structure taking into account the short-range magnetic order has made it possible to qualitatively explain the important experimental conclusion concerning the absence of a kink on the $\rho_{ab}(T)$ curves at the intersection with T_N. As regards the description of the temperature and concentration dependences of the conductivity and their anisotropy in the short-range magnetic order regime and the pseudogap generated by fluctuations of this magnetic order, qualitative analysis of experimental data shows the following role of the pseudogap in conduction. For strongly doped compositions with a large Fermi surface, all states participate in transport, and the conductivity anisotropy is insignificant (about 30). Upon a decrease in the carrier concentration and opening of a pseudogap near points $(\pi, 0)$ and $(0, \pi)$, the intraplanar conductivity decreases almost linearly upon an increase in the area of the Fermi surface covered by the pseudogap. The type of conductivity does not change in this case; consequently, the regions of the Fermi surface under the pseudogap simply do not contribute to the conductivity. For the conductivity along the c axis, the pseudogap in the region with the maximal dispersion immediately changes the conduction to the activation type partly shunted by the regions on the Fermi surface free of the pseudogap. The temperature dependence of the conductivity anisotropy is, accordingly, close to the activation-type dependence at high temperatures. Upon a decrease in temperature and the exponential decrease in the activation contribution to the interplanar conductivity, the role of the shunting regions increases, and anisotropy is saturated to values of about 10^4, at which the conductivity in all directions is controlled by the region of Fermi arches. In such a situation, we can expect an increase in anisotropy from 30 to approximately 10^4 both upon cooling and upon a decrease in the doping level at a fixed temperature; this is indeed observed in experiments. Comparison of the theoretical estimate (8) with experiment shows that, using single parameter y_0, we managed to describe the entire family of ρ_c/ρ_{ab} curves for various concentrations at high temperatures. We decided not to perform more complicated calculations by formula (6) with a Fermi surface depending on the doping level since our analysis of anisotropy is rough and qualitative in nature and does not claim to be a quantitative theory.

ACKNOWLEDGMENTS

This study was financially supported by the Russian Foundation for Basic Research (project nos. 09-02-01224 and 09-02-00127) and under the program "Quantum Physics of Condensed Media" of the Presidium of the Russian Academy of Sciences (project no. 5.7).

REFERENCES

1. N. F. Mott, *Metal–Insulator Transitions* (Taylor and Francis, London, 1974; Nauka, Moscow, 1979).
2. A. N. Lavrov and L. P. Kozeeva, Physica C (Amsterdam) **248**, 365 (1995); A. N. Lavrov and L. P. Kozeeva, Neorg. Mater. **34** (11), 1003 (1998) [Inorg. Mater. **34** (11), 1177 (1998)].
3. A. N. Lavrov, M. Yu. Kameneva, and L. P. Kozeeva, Phys. Rev. Lett. **81**, 5636 (1998).
4. Y. Ando, A. N. Lavrov, S. Komiya, K. Segawa, and X. F. Sun, Phys. Rev. Lett. **87**, 017001 (2001).
5. N. A. Kozlov and L. A. Maksimov, Zh. Éksp. Teor. Fiz. **48**, 1184 (1965) [Sov. Phys. JETP **21**, 790 (1965)].
6. Yu. V. Kopaev, Trudy Fiz. Inst. im. P. N. Lebedeva, Akad. Nauk SSSR **86**, 3 (1975).
7. D. I. Khomskii, Fiz. Met. Metalloved. **29** (1), 31 (1970) [Phys. Met. Metallogr. **29** (1), 31 (1970)].
8. E. V. Kuz'min and S. G. Ovchinnikov, Teor. Mat. Fiz. **31** (3), 379 (1977) [Theor. Math. Phys. **31** (3), 523 (1977)].
9. N. M. Plakida and V. S. Oudovenko, Zh. Éksp. Teor. Fiz. **131** (2), 259 (2007) [JETP **104** (2), 230 (2007)].
10. M. Imada, A. Fujimori, and Y. Tokura, Rev. Mod. Phys. **70**, 1039 (1998).
11. S. G. Ovchinnikov and O. G. Petrakovskii, Fiz. Tverd. Tela (Leningrad) **29** (6), 1866 (1987) [Sov. Phys. Solid State **29** (6), 1037 (1987)].
12. M. A. Kastner, R. J. Birgeneau, G. Shirane, and Y. Endoh, Rev. Mod. Phys. **70**, 897 (1998).
13. S. M. Hayden, G. Aeppli, H. Mook, D. Rytz, M. F. Hundley, and Z. Fisk, Phys. Rev. Lett. **66**, 821 (1991).
14. A. F. Barabanov, A. A. Kovalev, O. V. Urazaev, A. M. Belemuk, and R. Hayn, Zh. Éksp. Teor. Fiz. **119** (4), 777 (2001) [JETP **92** (4), 677 (2001)].
15. É. Z. Kuchinskii, I. A. Nekrasov, and M. V. Sadovskii, Pis'ma Zh. Éksp. Teor. Fiz. **82** (4), 217 (2005) [JETP Lett. **82** (4), 198 (2005)].
16. A. Damascelli, Z. Hussein, and Z. X. Shen, Rev. Mod. Phys. **75**, 473 (2003).
17. T. Ito, H. Takagi, S. Ishibashi, T. Ido, and S. Uchida, Nature (London) **350**, 596 (1991).
18. S. Komiya, Y. Ando, X. F. Sun, and A. N. Lavrov, Phys. Rev. B: Condens. Matter **65**, 214535 (2002).
19. K. Segawa and Y. Ando, Phys. Rev. B: Condens. Matter **69**, 104521 (2004).
20. A. N. Lavrov, L. P. Kozeeva, M. R. Trunin, and V. N. Zverev, Phys. Rev. B: Condens. Matter **79**, 214523 (2009).
21. A. N. Lavrov, Y. Ando, K. Segawa, and J. Takeya, Phys. Rev. Lett. **83**, 1419 (1999).

22. M. M. Korshunov and S. G. Ovchinnikov, Eur. Phys. J. B **57**, 271 (2007).
23. V. V. Val'kov and D. M. Dzebisashvili, Zh. Éksp. Teor. Fiz. **127** (3), 686 (2005) [JETP **100** (3), 608 (2005)].
24. S. G. Ovchinnikov, M. M. Korshunov, and E. I. Shneyder, Zh. Éksp. Teor. Fiz. **136** (5), 898 (2009) [JETP **109** (5), 775 (2009)].
25. H. Shimahara and S. Takada, J. Phys. Soc. Jpn. **60**, 2394 (1991); J. Phys. Soc. Jpn. **61**, 989 (1992).
26. A. F. Barabanov and V. M. Berezovskii, Zh. Éksp. Teor. Fiz. **106** (4), 1156 (1994) [JETP **79** (4), 627 (1994)].
27. V. V. Val'kov, T. A. Val'kova, D. M. Dzebisashvili, and S. G. Ovchinnikov, Pis'ma Zh. Éksp. Teor. Fiz. **75** (8), 450 (2002) [JETP Lett. **75** (8), 378 (2002)].
28. K. J. von Szczepanski P. Horsch, W. Stephan, and M. Ziegler, Phys. Rev. B: Condens. Matter **41**, 2017 (1990).
29. M. V. Sadovskii, Usp. Fiz. Nauk **171**, 539 (2001) [Phys.—Usp. **44** (5), 515 (2001)].
30. N. Doiron-Leyraud, C. Proust, D. LeBoeuf, J. Levallois, J.-B. Bonnemaison, R. Liang, D. A. Bonn, W. N. Hardy, and L. Taillefer, Nature (London) **447**, 565 (2007).
31. E. A. Yelland, J. Singleton, C. H. Mielke, N. Harrison, F. F. Balakirev, B. Dabrowski, and J. R. Cooper, Phys. Rev. Lett. **100**, 047003 (2008).
32. A. F. Bangura, J. D. Fletcher, A. Carrington, J. Levallois, M. Nardone, B. Vignolle, P. J. Heard, N. Doiron-Leyraud, D. LeBoeuf, L. Taillefer, S. Adachi, C. Proust, and N. E. Hussey, Phys. Rev. Lett. **100**, 047004 (2008).
33. X. J. Zhou, T. Yoshida, A. Lanzara, P. V. Bogdanov, S. A. Kellar, K. M. Shen, W. L. Yang, F. Ronning, T. Sasagawa, T. Kakeshita, T. Noda, H. Eisaki, S. Uchida, C. T. Lin, F. Zhou, J. W. Xiong, W. X. Ti, Z. X. Zhao, A. Fujimori, Z. Hussain, and Z.-X. Shen, Nature (London) **423**, 398 (2003).
34. W. J. Padilla, Y. S. Lee, M. Dumm, G. Blumberg, S. Ono, K. Segawa, S. Komiya, Y. Ando, and D. N. Basov, Phys. Rev. B: Condens. Matter **72**, 060511(R) (2005).
35. A. G. Loeser, Z. X. Shen, D. S. Dessau, D. S. Marshall, C. H. Park, P. Fournier, and A. Kapitulnik, Science (Washington) **273**, 325 (1996).
36. H. Ding, T. Yokoya, J. C. Campuzano, T. Takahashi, M. Randeria, M. R. Norman, T. Mochiku, K. Kadovaki, and J. Giapintzakis, Nature (London) **382**, 51 (1996).
37. J. W. Loram, J. Luo, J. R. Cooper, W. Y. Liang, and J. L. Tallon, J. Phys. Chem. Solids **62**, 59 (2001).
38. T. Yoshida, X. J. Zhou, H. Yagi, D. H. Lu, K. Tanaka, A. Fujimori, Z. Hussain, Z.-X. Shen, T. Kakeshita, H. Eisaki, S. Uchida, K. Segawa, A. N. Lavrov, and Y. Ando, Physica B (Amsterdam) **351**, 250 (2004).
39. V. Gavrichkov, A. Borisov, and S. G. Ovchinnikov, Phys. Rev. B: Condens. Matter **64**, 235124 (2001).
40. R. Hlubina and T. M. Rice, Phys. Rev. B: Condens. Matter **51**, 9253 (1995).
41. B. P. Stojkovic and D. Pines, Phys. Rev. B: Condens. Matter **55**, 8576 (1997).
42. L. B. Ioffe and A. J. Millis, Phys. Rev. B: Condens. Matter **58**, 11631 (1998).
43. A. T. Zheleznyak, V. M. Yakovenko, and H. D. Drew, Phys. Rev. B: Condens. Matter **59**, 207 (1999).
44. A. Perali, M. Sindel, and G. Kotliar, Eur. Phys. J. B **24**, 87 (2001).
45. N. M. Plakida, Z. Phys. B: Condens. Matter **103**, 383 (1997).
46. G. Jackeli and N. M. Plakida, Phys. Rev. B: Condens. Matter **60**, 5266 (1999).
47. A. M. Belemuk, A. F. Barabanov, and L. A. Maksimov, Zh. Éksp. Teor. Fiz. **129** (3), 493 (2006) [JETP **102** (3), 431 (2006)].
48. A. M. Belemuk, A. F. Barabanov, and L. A. Maksimov, Pis'ma Zh. Éksp. Teor. Fiz. **86** (5), 374 (2007) [JETP Lett. **86** (5), 321 (2007)].

Translated by N. Wadhwa